Article

Cell Reports

Tissue-Resident CD169^{+} Macrophages Form a Crucial Front Line against *Plasmodium* Infection

Graphical Abstract

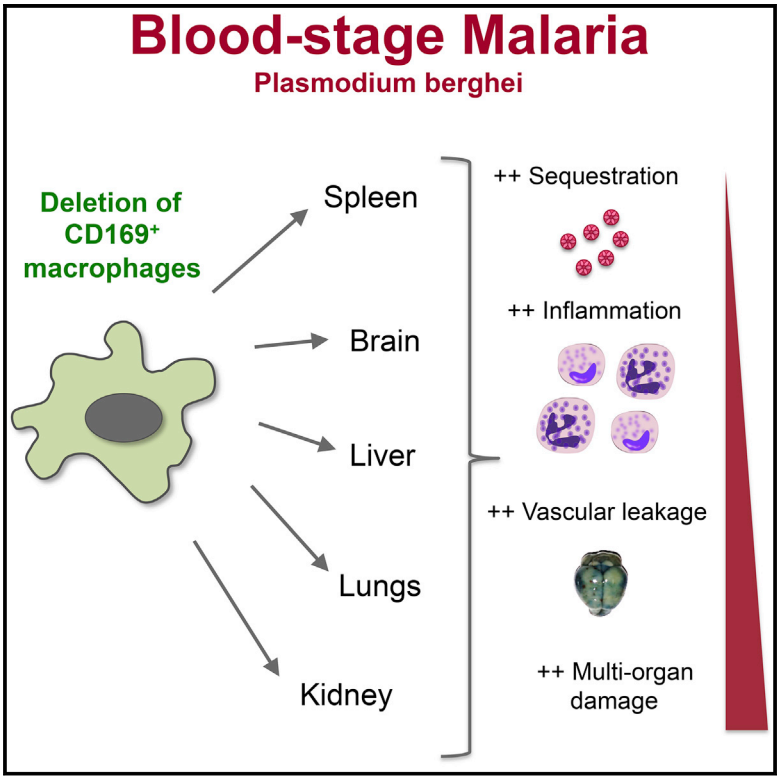

Authors

Pravesh Gupta, Si Min Lai, Jianpeng Sheng, ..., Laurent Renia, Klaus Karjalainen, Christiane Ruedl

Correspondence

ruedl@ntu.edu.sg

In Brief

Using an animal model of blood-stage malaria, Ruedl et al. demonstrate that a distinct innate immune cell type, the tissue-resident CD169^{+} macrophage, controls parasite propagation and sequestration and restrains inflammation. In the absence of these macrophages, *Plasmodium* infection is lethal in the model as a result of multiple organ damage.

Highlights

- CD169^{+} macrophages can control parasite propagation and restrain inflammation
- Lack of CD169^{+} macrophages augments hemozoin deposition in several organs
- Vascular leakage in CD169-DTR mice occurs during malaria
- *Plasmodium* infection leads to multi-organ damage in absence of CD169^{+} macrophages

Gupta et al., 2016, Cell Reports *16*, 1749–1761
August 9, 2016 © 2016 The Author(s).
http://dx.doi.org/10.1016/j.celrep.2016.07.010

Cell Reports
Article

OPEN ACCESS
CellPress

Tissue-Resident CD169$^+$ Macrophages Form a Crucial Front Line against *Plasmodium* Infection

Pravesh Gupta,[1] Si Min Lai,[1,2] Jianpeng Sheng,[1] Piotr Tetlak,[1] Akhila Balachander,[2] Carla Claser,[2] Laurent Renia,[1,2] Klaus Karjalainen,[1] and Christiane Ruedl[1,*]
[1]Nanyang Technological University, School of Biological Sciences, 60 Nanyang Drive, Singapore 637551, Singapore
[2]Singapore Immunology Network, Agency for Science, Technology and Research (A*STAR), 8A Biomedical Grove, Singapore 138648, Singapore
*Correspondence: ruedl@ntu.edu.sg
http://dx.doi.org/10.1016/j.celrep.2016.07.010

SUMMARY

Tissue macrophages exhibit diverse functions, ranging from the maintenance of tissue homeostasis, including clearance of senescent erythrocytes and cell debris, to modulation of inflammation and immunity. Their contribution to the control of blood-stage malaria remains unclear. Here, we show that in the absence of tissue-resident CD169$^+$ macrophages, *Plasmodium berghei* ANKA (PbA) infection results in significantly increased parasite sequestration, leading to vascular occlusion and leakage and augmented tissue deposition of the malarial pigment hemozoin. This leads to widespread tissue damage culminating in multiple organ inflammation. Thus, the capacity of CD169$^+$ macrophages to contain the parasite burden and its sequestration into different tissues and to limit infection-induced inflammation is crucial to mitigating *Plasmodium* infection and pathogenesis.

INTRODUCTION

During malaria, myeloid cells, such as monocytes, macrophages, and dendritic cells (DCs), play key roles in both innate and adaptive host defense strategies. Macrophages, as professional phagocytic cells, remove infected erythrocytes and cellular debris, whereas DCs are highly specialized to prime strong T cell responses (Cockburn and Zavala, 2016). DCs and macrophages located in the spleen are of particular importance in parasite clearance and the orchestration of the host immune response (Wykes et al., 2007). Indeed, removal of *Plasmodium*-infected red blood cells (iRBCs) and generation of parasite-specific immunity occurs predominantly within the spleen. Splenectomized humans and mice with acute malaria exhibit a reduced capacity for iRBC clearance as well as a diminished anti-parasite immune response, leading to a higher peak of parasitemia (Bach et al., 2005; Weiss, 1989).

Along with tissue-resident red pulp macrophages, marginal zone macrophages (MZM) and marginal metallophilic macrophages (MMM), which are positioned strategically at the outer boundary of the splenic marginal zone next to the red pulp, play an important role in the clearance of iRBCs during malaria (Engwerda et al., 2005b). iRBCs display decreased deformability as they age and are therefore easily trapped in the red pulp reticular network where they can be phagocytosed and cleared (Cooke et al., 2004; Sherman et al., 2004). During the acute stage of *Plasmodium* infection, the splenic microarchitecture is dramatically disrupted (Weiss, 1989) as a result of a massive recruitment of bone marrow-derived myeloid cells, including CD11b^{hi}Ly6C^{hi} inflammatory monocytes, which are particularly important in controlling blood-stage malaria parasites, such as *P. chabaudi* (Sponaas et al., 2009).

It is essential that the immune response during malaria is tightly controlled and regulated. Excessive and inappropriate immune activation can lead to severe overlapping pathologies, such as cerebral malaria (Schofield and Grau, 2005), acute lung injury (ALI), and acute respiratory distress syndrome (ARDS) (Taylor et al., 2006). However, the exact cellular mechanisms leading to these different pathologies remain unclear. We have recently demonstrated the contribution of cross-priming Clec9A (DNGR-1)$^+$ DCs to the activation of a parasite-specific cytotoxic T cell response, which can lead to severe acute cerebral pathology (Piva et al., 2012).

Here, we investigate the contribution of tissue-resident CD169$^+$ macrophages in parasite clearance and immunopathology during *P. berghei* ANKA (PbA) infection. This macrophage subset is strategically localized at sites of *Plasmodium*-infected red blood cells entry such as splenic marginal zone or liver sinusoids. Using a CD169-diphtheria toxin receptor (DTR) transgenic mouse line, in which CD169$^+$ macrophages are specifically ablated following application of diphtheria toxin (DT), enabled us to study the role of these cells in vivo, not only in the spleen, but also in other organs, such as the liver, lungs, and kidneys. Mice lacking resident macrophages showed abnormally high levels of sequestered parasites, leading to increased levels of hemozoin (Hz) deposits and to an augmented recruitment of inflammatory cells in all tested organs. Consequently, CD169-DTR mice were subject to dramatically increased immunopathology, culminating in multiple organ damage.

RESULTS

Specific Ablation of Tissue-Resident Macrophages in CD169-DTR Mice

CD169 is a lectin-like receptor whose expression is restricted to tissue-resident macrophages, inclusive F4/80^{hi}CD11b^{int} cells,

This is an open access article under the CC BY-NC-ND license (http://creativecommons.org/licenses/by-nc-nd/4.0/).

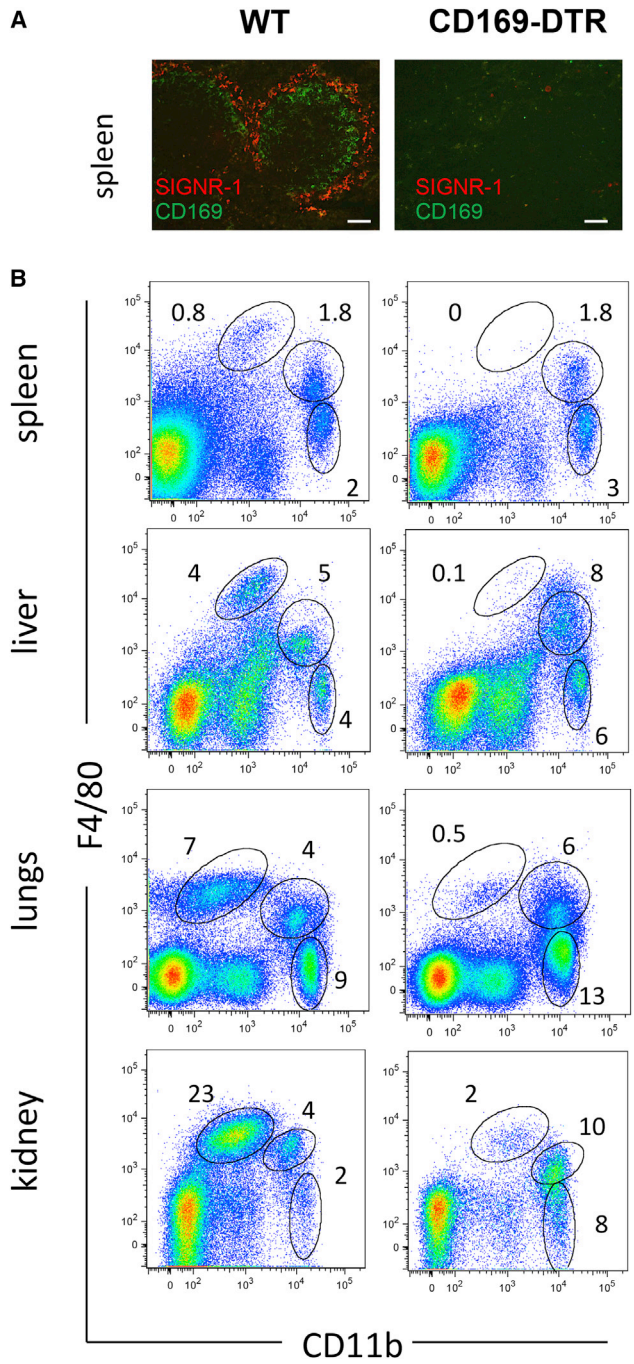

Figure 1. Tissue-Resident Macrophages Are Effectively Ablated in the Spleen, Liver, Lungs, and Kidneys of DT-Treated CD169-DTR Mice

(A) Immunofluorescence staining of SIGN-R1^{+} MZM and CD169^{+} MMM in the spleen of WT and CD169-DTR mice. Cryostatic sections (6 μm) of spleens were stained with biotinylated-anti SIGNR-1/Texas Red-Streptavidin and FITC-anti CD169. Magnification: 20×.

(B) Flow cytometric analysis of single cell suspensions from the spleen, liver, lungs, and kidneys of WT and DT-injected CD169-DTR mice showing effective depletion of F4/80^{hi} CD11b^{int} macrophages in CD169-DTR mice. WT BALB/c and CD169-DTR mice were injected i.p. at day −2 and −1 with 10 ng/g DT and analyzed at day 0. Representative dot plots of cells obtained from three mice are shown and results were confirmed in three independent experiments. Numbers show the percentage of each gated myeloid cell subset (tissue-resident macrophages (F4/80^{hi} CD11b^{int}), monocyte-derived macrophages (F4/80^{int} CD11b^{hi}), and neutrophils (F4/80^{neg} CD11b^{hi}).

See also Figures S1 and S5.

present in various organs and tissues (Figures 1 and S1A). The micro-anatomical localization of CD169^{+} macrophage in the splenic marginal zone area (Figure 1A), within the hepatic sinusoids as well as close to vasculature in brain and kidneys (Figure S1B), suggests their importance as frontline sentinels in removing particulate blood-borne antigens, such as parasitized erythrocytes. To probe the potential function of tissue-resident macrophages during *Plasmodium* infection, we first confirmed that we were able to ablate tissue-resident macrophages, i.e., CD169^{+} cells, but not infiltrating monocytic/macrophage cells (F4/80^{int}CD11b^{hi}) or neutrophils (F4/80^{neg}CD11b^{hi}), in DT-injected CD169-DTR but not in DT-injected WT mice (hereafter referred to as CD169-DTR and wild-type [WT], respectively) (Purnama et al., 2014; Schulz et al., 2012; Sheng et al., 2015). Two DT injections (day −2 and −1 before analysis) led to a rapid and efficient ablation of red pulp macrophages in the spleen, Kupffer cells in the liver, lung alveolar and kidney-resident macrophages, as well as MZMs and MMMs (Figures 1A and 1B) and the depletion of CD169-expressing cells could be maintained during the infection by DT injections every 3–4 days (Figure S1B). Note that the disappearance of MZMs is the consequence of structural changes to the marginal zone due to the ablation of MMMs and is not a direct effect of DT in those cells.

CD169-DTR Mice Are More Susceptible to PbA Infection

The course of PbA infection was monitored in control WT (BALB/c) and CD169-DTR (BALB/c) mice. Both mouse strains were treated with DT (day −2 and −1 pre-infection and subsequently every 3–4 days), and infected with PbA-GFP (day 0). Survival and circulating parasitemia was monitored and recorded over a period of 25 days. As shown in Figure 2A, parasitemia developed steadily to day 8 in WT mice and, after a short 2-day plateau, increased sharply over the following 3 days (days 11–14), reaching a final plateau with 55%–60% of iRBCs. The high level of iRBCs resulted in reduced survival in WT control mice from day 16 post-infection due to anemia as evident by reduction of RBC and hemoglobin levels (Figure S2A). The course of disease differed substantially in DT-treated CD169-DTR mice, in which the proportion of infected RBCs peaked at just 20%, before declining sharply again after day 9. This was followed by the rapid death of all CD169-DTR mice (Figure 2A). Similar premature deaths and higher parasitemia levels were also observed with CD169-DTR mice infected with non-lethal *P. yoelii* 17XNL (Figure S2C).

We considered that the differences in parasitemia in the circulation might reflect altered parasite sequestration. To gain further insights into the dynamics of parasite sequestration within our model, we performed real-time in vivo parasite imaging from day 6–9 post infection. WT and CD169-DTR mice were infected with PbA expressing the bioluminescent reporter luciferase (PbALuc) to allow visualization and quantification of sequestered iRBCs in different organs, including the spleen, brain, liver, lungs,

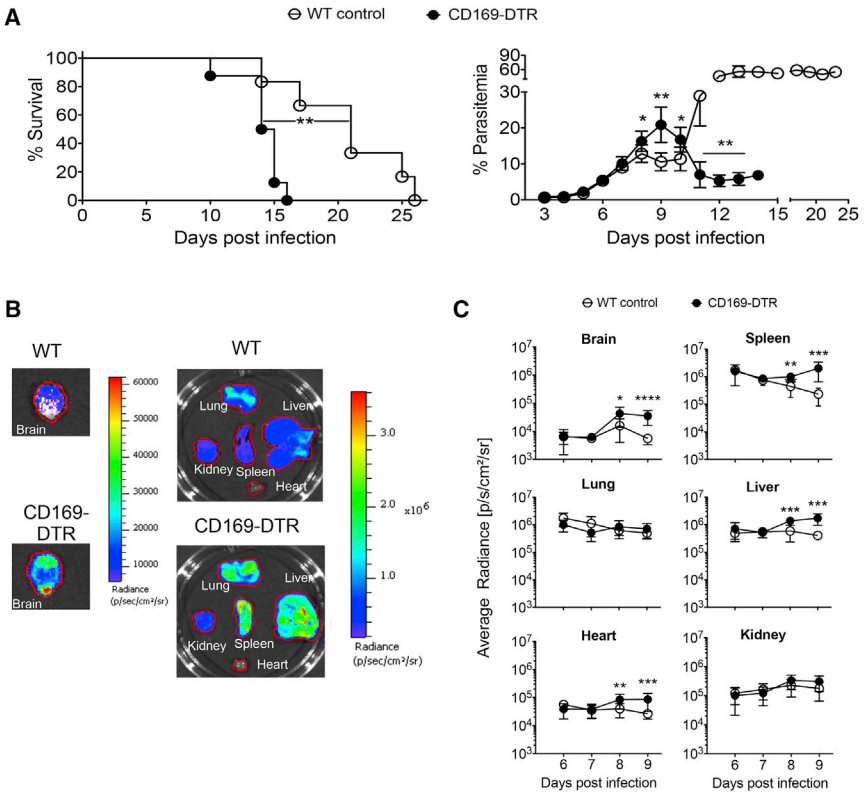

Figure 2. Mice Are More Susceptible to PbA Infection and Show Higher Parasite Burdens in the Absence of Tissue-Resident Macrophages

(A) Survival (left) and parasitemia (right) of 6- to 8-week-old PbA-infected WT controls (white circles) and CD169-DTR mice (black circles) (n = 6–8/group). Statistical significance of survival was analyzed using the Mantel-Cox log-rank test and statistical significance of parasitemia was determined using a Mann-Whitney U test. Data are cumulative of two independent experiments.

(B and C) Quantification of in vivo bioluminescence imaging of iRBCs in the indicated organs of PbA-infected WT and CD169-DTR mice. (B) Pseudocolor images of brain, spleen, liver, lungs, kidneys, and heart collected from a representative PbA-infected WT and CD169-DTR mouse on day 9. (C) Daily bioluminescence imaging (from day 6–9 post infection) during PbA infection. Each point represents the mean average radiance (p/s/cm^2/sr) values (log) ± SD of 6–9 mice. White circles, WT; black circles, CD169-DTR mice. Statistical significance was determined using an unpaired Student's t test. *$p < 0.05$, **$p < 0.01$, ***$p < 0.001$. Data are cumulative of two independent experiments. See also Figure S2.

heart, and kidneys (Claser et al., 2011). A representative set of organs collected from WT and CD169-DTR mice at day 9 post-infection is shown in Figure 2B. We observed a significant increase in the levels of sequestered iRBCs over time in the spleen, brain, heart, and liver of CD169-DTR mice (Figures 2C and S2B), which suggests that the sharp decrease of parasitemia in the circulation of CD169-DTR mice is in fact due to a massive sequestration of iRBCs into the tissues.

Dysregulated Immune Response and Increased Splenic Immunopathology in PbA-Infected CD169-DTR Mice

In blood-stage malarial infection, the spleen is the major immune organ involved not only in mounting innate and adaptive antimalarial responses, but also in providing effective filtration and removal of iRBCs. To examine the contribution of specialized splenic macrophage subpopulations, such as MZMs, MMMs, and red pulp CD169$^+$ macrophages to this process, we infected WT and CD169-DTR mice with PbA and analyzed their spleens at day 6 and 8 post infection by histopathology and flow cytometry for changes in structure and cell populations.

Histological analysis of the spleens from infected WT mice (day 8) revealed that marginal zone atrophy had occurred, leaving a clear zone of white pulp. The red pulp was expanded by extramedullary hematopoiesis with a moderate infiltration of myeloid cells and a mild deposition of Hz pigment. The sinuses were distended with blood containing some parasitized red blood cells (Figure 3A, left panels). CD169-DTR mice showed a different picture. The MZs had collapsed, as evidenced by the fusion of white pulp, with lymphoid hyperplasia, to the adjacent red pulp. The red pulp was clearly expanded with marked lymphoid and myeloid infiltration, mild EMH, and pronounced Hz pigment deposition. The sinuses were moderately distended with blood cells containing a high proportion of iRBCs (Figures 3A, right panels, and S3). Comparison of spleen sections from uninfected control and ablated CD169-DTR mice are shown in Figure S2D.

Flow cytometry analysis confirmed the enhanced recruitment of both monocyte-derived Ly6C^{hi} cells as well as Ly6G^{hi} neutrophils to the CD169-DTR spleens (Figure 3C). However, CD8$^+$ T cells from ablated mice showed lower expression of the early activation marker CD69 and granzyme B and decreased numbers of IFN-γ-producing CD4$^+$ as well as CD8$^+$ T cells were detected in the spleen of CD169-DTR mice (Figure 3D). This reduction in IFN-γ-producing cells was reflected in lower levels of IFN-γ in the serum of CD169-DTR mice (Figure 3B).

Cerebral Pathology in CD169-DTR Mice in Response to PbA Infection

Generally, BALB/c mice infected with PbA are considered resistant to experimental cerebral malaria (ECM) (Engwerda et al., 2005a) because they do not develop clear neurological symptoms or brain damage (Figures 4A–4C). These mice typically survive the ECM window and die as a result of the complications of hyperparasitemia (Figures 2A and S2A). Indeed, blood vessels in the brain parenchyma and meninges of infected control WT mice (day 8 post infection) did not show histological manifestations of ECM. However, in CD169-DTR mice, a prominent intravascular

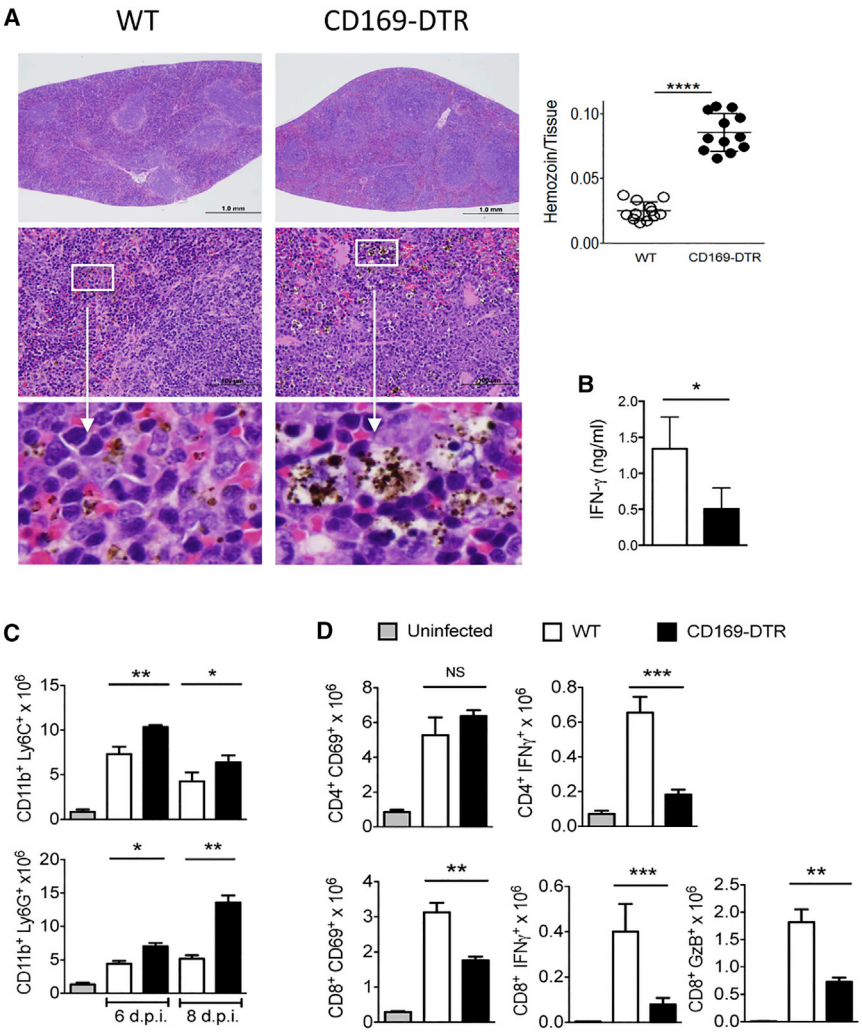

Figure 3. Histological and Cellular Analysis of Spleens WT and CD169-DTR Mice after PbA Infection

(A) Representative histological H&E sections from the spleens of WT and CD169-DTR mice on day 8 post PbA infection. Scale bars, 1 mm (upper panel) and 100 μm (middle panels). Lower panels show magnification of areas to depict Hz deposits. Dot chart shows the quantification of Hz in the spleen of control (white circles) and CD169-DTR mice (black circles), ****$p < 0.0001$.

(B) Mean of IFN-γ ± SD measured in the serum of WT (white bars) and CD169-DTR (black bars) infected with PbA at day 8 (n = 4–8 mice/group). Statistical significance was determined using an unpaired Student's t test. *$p < 0.05$, **$p < 0.01$, ***$p < 0.001$.

(C) Augmented numbers of inflammatory Ly6C^{hi} and Ly6G^{hi} cells in the spleen of PbA-infected CD169-DTR mice. Bar charts represent mean absolute numbers ± SD of Ly6C^{hi} and Ly6G^{hi} cells in the spleens of uninfected (gray bars), infected WT (white bars), and infected CD169-DTR mice (black bars) at days 6 and 8 post infection (n = 4/group). Statistical significance was determined using an one-way ANOVA followed by Bonferroni test.

(D) Bar charts represent mean absolute numbers ± SD of CD69$^+$CD4$^+$ and CD69$^+$CD8$^+$ T cells (gated on CD3$^+$), as well as IFN-γ-producing CD4$^+$ T cells and Granzyme B-expressing CD8$^+$ T cells, in the spleens of uninfected WT (gray bars), infected WT (white bars), and infected CD169-DTR mice (black bars) at day 8 post infection (n = 4/group). Statistical significance was determined using a one-way ANOVA followed by Bonferroni test. Results were confirmed in two independent experiments.

See also Figures S2 and S5.

accumulation of leukocytes and iRBCs was detectable in the lumen of most blood vessels of the brain, as well as augmented granular brown Hz pigment. Quantification of Hz in histological sections of brains collected at day 8 post-infection confirmed the increased deposition of Hz observed in classical histology (Figures 4D and S3). In addition, multifocal areas of hemorrhage, seen predominantly in the cerebellar parenchyma, were clearly apparent in CD169-DTR mice (Figures 4A–4C). Consistent with our histological findings, CD169-DTR mice developed obvious neurological symptoms of ECM, such as ataxia, loss of grip strength, and progressive paralysis, as evaluated by the Rapid Murine Coma and Behavior Scale (RMCBS) although less pronounced when compared to the highly ECM-susceptible mouse strain C57BL/6J (Figure 4E). Flow cytometry revealed abundant inflammatory monocyte, neutrophil, and lymphoid CD4$^+$ and CD8$^+$ T cell sequestration (Figures 4F–4H) in the brains of CD169-DTR mice. Recruited CD4$^+$ and CD8$^+$ T cells in particular showed clear evidence of activation, with elevated production of IFN-γ and granzyme B, respectively (Figure 4H). In addition, the integrity of the blood-brain barrier (BBB) was compromised in CD169-DTR mice, as demonstrated by leakage of Evans blue dye into the brain tissue (Figure 4I).

Increased Inflammatory Cell Infiltrates, Vascular Leakage, and Deposition of Hz in the Liver, Lungs, Kidneys, and Heart upon PbA Infection in the Absence of Tissue-Resident Macrophages

Liver-resident immune cells are also thought to play a key role in blood-stage malaria, promoting effective anti-malarial effector mechanisms (Wunderlich et al., 2014). Because liver Kupffer cells, known to be efficient in iRBC clearance (Murthi et al., 2006), are CD169$^+$, we examined the consequences of Kupffer cell ablation on liver pathology following PbA infection. At days 6 and 8 post infection, similar to our findings in the spleen and lung, the activation and effector status of both CD8$^+$ and CD4$^+$ T cells was attenuated in the livers of CD169-DTR mice (Figure 5A), and the recruitment of inflammatory monocytes and neutrophils was increased (Figure 5B). Consistent with this, histological analysis of the livers of CD169-DTR mice revealed an increase in sinusoid cellularity due to mononuclear cell

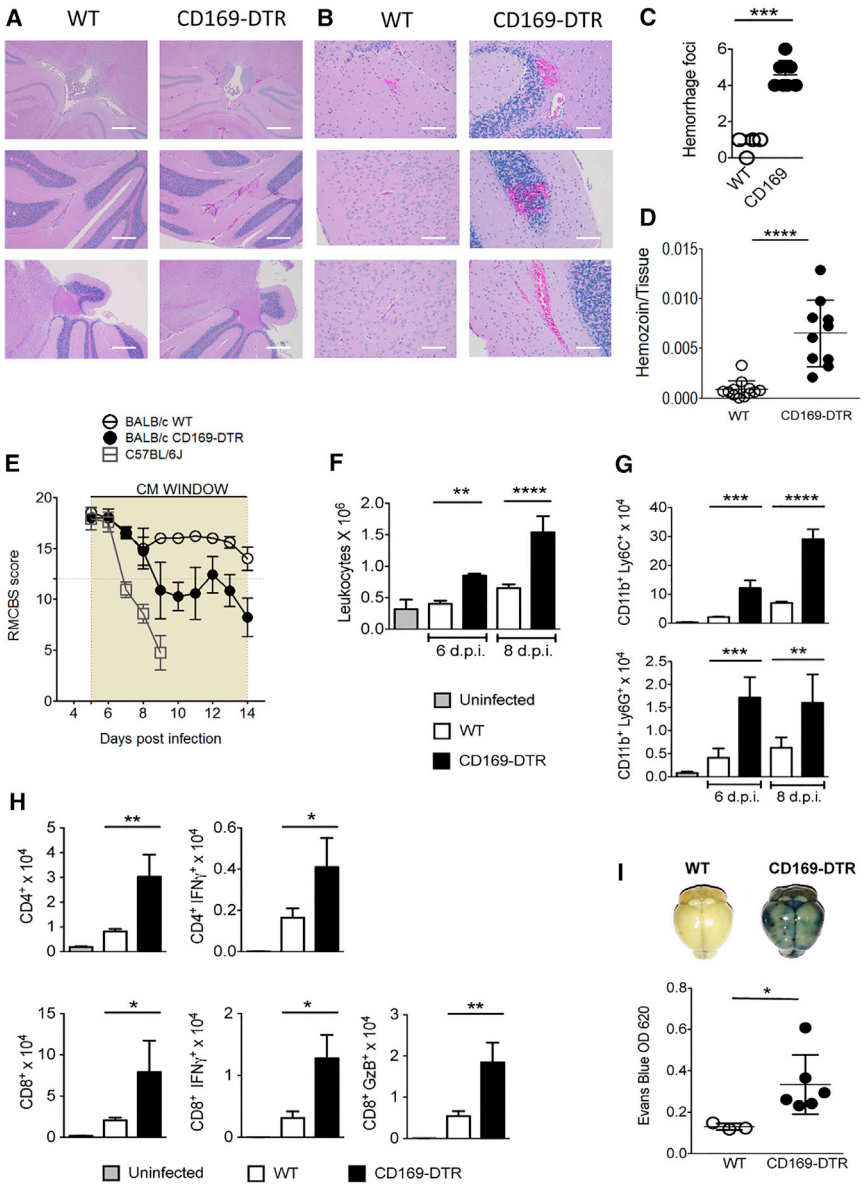

Figure 4. PbA Infection Causes ECM in CD169-DTR Mice

(A and B) Representative histological H&E sections from brains of WT and symptomatic CD169-DTR mice at day 8 post infection. Intravascular sequestration of iRBCs and leukocytes with local hemorrhagic foci are only detected in the brains of CD169-DTR mice. Scale bars, 500 μm (left panels) (A) and 100 μm (right panels) (B). Images are representative of two independent experiments.

(C) Mean number of hemorrhagic foci ± SD per brain in WT and CD169-DTR mice (n = 5–6 mice/group). Statistical significance was determined using an unpaired Student's t test.

(D) Dot chart shows the quantification of Hz in the brain of control (white circles) and CD169-DTR mice (black circles) ****$p < 0.0001$.

(E) Severity of ECM determined by RMCBS scoring in WT and CD169-DTR mice (n = 8/group) infected with PbA-GFP, dash line indicates the threshold scores below which mice show distinct neurological signs characteristic of ECM. RMCBS values of the ECM-susceptible C57BL/6 mouse strain are included. Data are cumulative of two independent experiments.

(F) Augmented cellular sequestration of total leukocytes in infected CD169-DTR brains (black bars) compared with uninfected (gray bars) and PbA-infected WT mice (white bars) (n = 4/group). Data are represented as mean ± SD. Statistical significance was determined using an one-way ANOVA followed by Bonferroni test.

(G) Augmented accumulation of inflammatory Ly6C^{hi} and Ly6G^{hi} cells in the brain of PbA-infected CD169-DTR mice. Total numbers of Ly6C^{hi} and Ly6G^{hi} cells (gated on CD45^{hi} cells) in the brains of uninfected (gray bars), infected WT (white bars), and infected CD169-DTR mice (black bars) at days 6 and 8 post infection (n = 4/group). Data are represented as mean ± SD. Statistical significance was determined using an one-way ANOVA followed by Bonferroni test.

(H) Enhanced brain-sequestered effector CD4$^+$ and CD8$^+$ T cells in CD169-DTR mice. Total numbers of brain-sequestered CD4$^+$ and CD8$^+$ T cells (gated on CD3$^+$), as well as IFN-γ-producing CD4$^+$ T cells and Granzyme B-expressing CD8$^+$ T cells, in uninfected (gray bars), infected WT (white bars), and infected CD169-DTR mice (black bars) (n = 4/group, day 8). Statistical significance was determined using an one-way ANOVA followed by Bonferroni test.

(I) Blood-brain barrier integrity in PbA-infected WT and CD169-DTR mice. At day 9 post infection, mice were injected with 0.1% Evans blue dye 60 min prior to dissection. Representative images of brains from PbA-infected WT and CD169-DTR are shown. Evans blue dye was extracted from brains using formamide, and absorption of the extract was measured at 620 nm (n = 3–6/group). Data are represented as mean ± SD. Statistical significance was determined using an unpaired Student's t test. *$p < 0.05$, **$p < 0.01$, ***$p < 0.001$, ****$p < 0.0001$. Data shown in (F) to (H) are representative of two independent experiments.

See also Figures S3 and S5.

infiltration, which was less prominent in WT mice (Figure 5C, upper panels). Furthermore, elevated amounts of Hz were detected in the livers of PbA-infected CD169-DTR mice with distinct large black-brown pigment deposits distinguishable in the vasculature as well as throughout the hepatic tissue (Figures 5C and S3). Because high parasite burdens are known to cause tissue injury, we analyzed serum levels of the liver enzyme, alanine transaminase (ALT), as a parameter of liver damage. As shown in Figure 5D, CD169-DTR mice showed high ALT levels indicative of liver damage as early as day 6 post infection, whereas the ALT levels of PbA-infected control mice were minimally increased. Liver damage was further confirmed by histological analysis of collagen using picrosirius red (PSR) staining. Liver sections of CD169-DTR, but not WT mice, showed evidence of mild liver fibrosis with collagen fibers detectable not only at the blood vessels but also within the liver parenchyma (Figure 5E). Furthermore, CD169-DTR mice had markedly increased vascular permeability in the liver on day 8

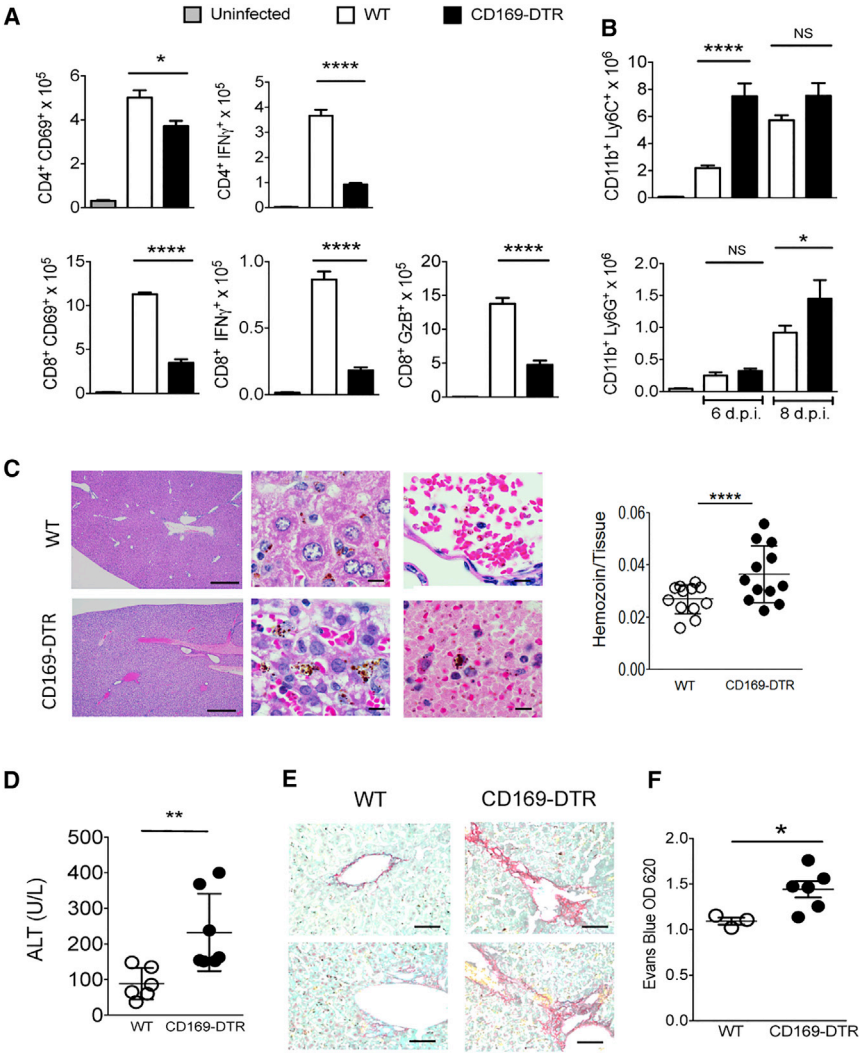

Figure 5. Depletion of Kupffer Cell Leads to Malaria-Induced Liver Damage

(A) Liver effector $CD4^+$ and $CD8^+$ T cells in PbA-infected WT and CD169-DTR mice. Bar charts represent mean total numbers ± SD of $CD69^+CD4^+$ and $CD69^+CD8^+$ T cells (gated on $CD3^+$), as well as well as IFN-γ-producing $CD4^+$ T cells and Granzyme B-expressing $CD8^+$ T cells, in the liver of uninfected WT (gray bars), infected WT (white bars), and infected CD169-DTR mice (black bars) at day 8 post infection. (n = 4/group). Statistical significance was determined using an one-way ANOVA followed by Bonferroni test.

(B) Augmented infiltration of inflammatory $Ly6C^{hi}$ and $Ly6G^{hi}$ cells in the livers of PbA-infected CD169-DTR mice at days 6 and 8 post infection. Bar chart represents mean total numbers ± SD of $Ly6C^{hi}$ and $Ly6G^{hi}$ cells in the livers of uninfected (gray bars), infected WT (white bars), and infected CD169-DTR mice (black bars) (n = 4/group). Statistical significance was determined using an one-way ANOVA followed by Bonferroni test.

(C) Representative H&E-stained liver sections of PbA-infected WT and CD169-DTR mice at day 8 post infection. Scale bars, 500 μm (left panels) and 10 μm (right panels). Pictures on the right-hand side show magnification of areas to depict Hz deposits. Dot chart shows the quantification of Hz in the liver of control (white circles) and CD169-DTR mice (black circles).

(D) Serum alanine transaminase (ALT) levels of WT (white circles) and CD169-DTR mice (black circles). Values represent mean ALT levels ± SD in units/L (n = 7/group). Statistical significance was determined using an unpaired Student's t test. Data shown are cumulative of two independent experiments.

(E) Representative images of picrosirius red staining for collagen visualization in the livers of PbA-infected WT and CD169-DTR mice. Scale bars, 50 μm.

(F) Vascular permeability in the liver is increased in CD169-DTR mice. Values represent the mean optical density ± SD of Evans blue dye extracts measured at 620 nm (n = 3–6/group). Statistical significance was determined using an unpaired Student's t test. *p < 0.05, **p < 0.01, ***p < 0.001, ****p < 0.0001. Data shown in (A), (B), (C), and (E) are representative of two independent experiments.
See also Figures S3 and S5.

post PbA infection, as assessed by Evans blue dye extrusion (Figure 5F).

Malaria-associated ALI and its acute severe form, ARDS, are often life-threatening pulmonary complications of malaria, and their pathophysiology is not completely understood. To investigate the role of alveolar macrophages in the pathology of PbA infection in the respiratory tract, we analyzed lung lavage (day 6) and lung tissue collected at day 6 and 8 post infection. Macroscopically, the lungs of CD169-DTR mice were noticeably darker in color, suggestive of enhanced Hz pigment accumulation in the lung tissue (Figure 6A). Histological analysis confirmed marked Hz pigment deposition in the interstitial tissue of CD169-DTR mouse lung sections, not present in WT mice (Figures 6B and S3). Flow cytometry profiling of the lung revealed similar trends to the spleen. Recruitment of inflammatory monocytes and neutrophils was increased in the lungs of CD169-DTR mice, while the proportion of IFN-γ or Granzyme B-positive T cells was reduced (Figures 6C and 6D). In addition, the alveolar-capillary membrane barrier was compromised in infected CD169-DTR mice, evidenced by the markedly increased IgM and IgG leakage into the bronchoalveolar lavage (BAL) fluid (Figure 6E).

Events in the kidneys and heart mirrored those occurring in the spleen, lungs, and liver during PbA infection. Increased infiltration of inflammatory cells (Figures S4A and S4B) and marked vascular leakage were also observed in these organs in CD169-DTR mice (Figure S4C).

Tissue-Resident $CD169^+$ Macrophages Have Anti-inflammatory Properties Characterized by High IL-10 Production

Serum levels of pro-inflammatory TNF-α and anti-inflammatory IL-10 cytokines were monitored during the course of PbA infection in control and CD169-DTR mice. IL-10 serum levels

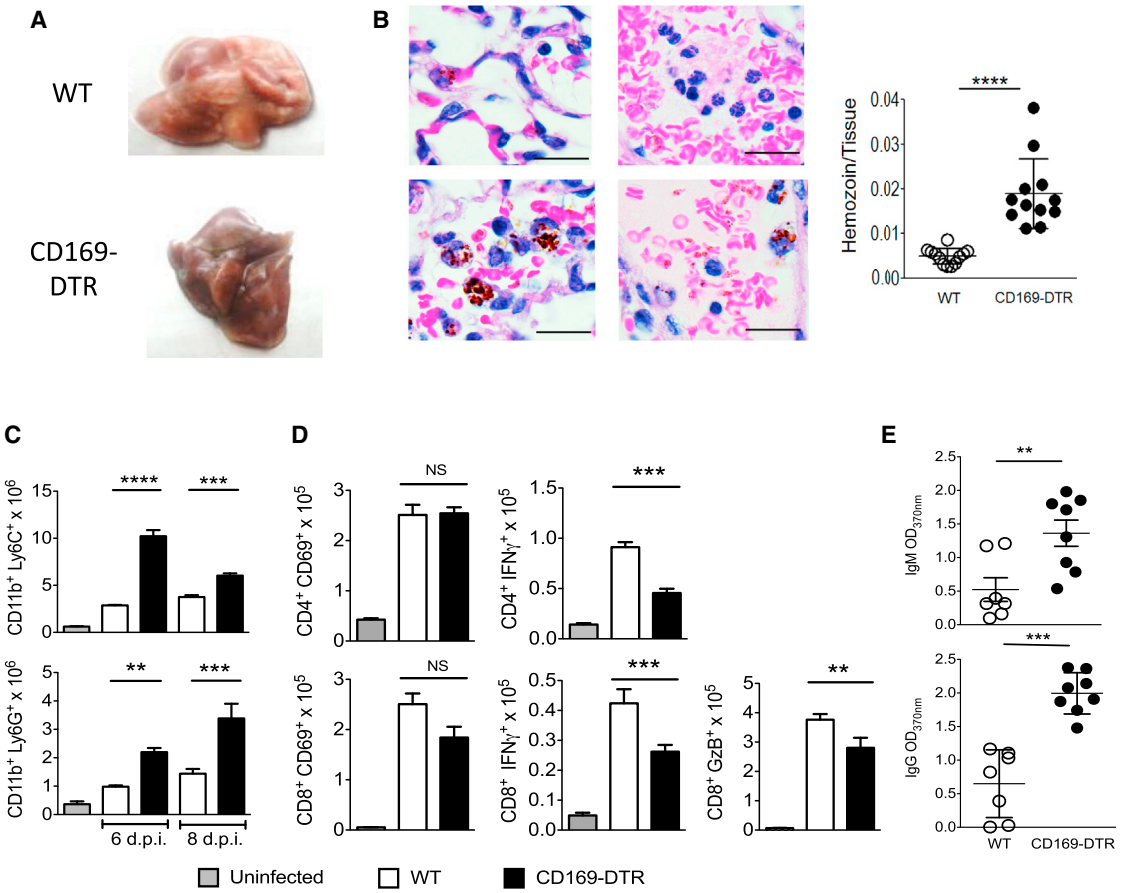

Figure 6. PbA Infection Causes Lung Inflammation and Pathology in CD169-DTR Mice

(A) Macroscopic view of lungs collected from PbA-infected WT and CD169-DTR mice (day 8 post infection).

(B) Representative histological H&E sections show clear large Hz deposits in CD169-DTR mice. Scale bars, 10 μm. Dot chart shows the quantification of Hz in the lungs of control (white circles) and CD169-DTR mice (black circles).

(C) Augmented infiltration of inflammatory Ly6C^{hi} and Ly6G^{hi} cells in the lungs of PbA-infected CD169-DTR mice. Bar chart represents mean total number ± SD of Ly6C^{hi} and Ly6G^{hi} cells in lungs of uninfected (gray bars), infected WT (white bars), and infected CD169-DTR mice (black bars) at days 6 and 8 post infection (n = 4/group). Statistical significance was determined using an one-way ANOVA followed by Bonferroni test.

(D) Lung effector CD4$^+$ and CD8$^+$ T cells in WT and CD169-DTR mice. Bar charts represent mean total numbers ± SD of CD69$^+$CD4$^+$ and CD69$^+$CD8$^+$ T cells (gated on CD3$^+$), as well as IFN-γ-producing CD4$^+$ T cells and Granzyme B-expressing CD8$^+$ T cells, in lungs of uninfected WT (gray bars), infected WT (white bars), and infected CD169-DTR mice (black bars) at day 8 post infection. (n = 4/group). Statistical significance was determined using an one-way ANOVA followed by Bonferroni test.

(E) Determination of IgM and IgG levels by ELISA in bronchoalveolar lavage (BAL) fluid as biomarkers for pulmonary vascular leakage. BAL was collected from PbA-infected WT (white circles) and CD169 DTR mice (black circles) at day 6 post infection. Data are represented as mean optical density ± SD (n ≥ 7/group). Statistical significance was determined using an unpaired Student's t test. **p < 0.01, ***p < 0.001, ****p < 0.0001. Data shown are cumulative of two independent experiments.

Data shown in (C) and (D) are representative of two independent experiments. See also Figure S3.

gradually increased with the progression of the infection in both groups although CD169-DTR mice had significantly lower levels while the serum abundance of TNF-α showed just the opposite trend (Figure 7A, left) indicating a pronounced inflammation in mice lacking CD169$^+$ macrophages.

Having detected a low IL-10/TNF ratio in the serum of CD169-DTR mice during PbA infection, we aimed to determine the involvement of F4/80^{high}CD169$^+$ macrophages in IL-10 production. In uninfected mice, comparison of CD169$^+$ macrophages to lymphocytes (Figure 7B) and other myeloid cells, such as the tissue-infiltrating Ly6C^{high} monocytes revealed that this macrophage subset has intrinsic anti-inflammatory properties, characterized by enhanced IL-10 production and reduced mRNA levels of inflammatory cytokines such as TNF-α (Figure 7C). This anti-inflammatory phenotype was maintained during PbA infection because CD169$^+$ macrophages isolated from infected livers showed similar IL-10 expression profile when compared to macrophages isolated from uninfected mice. On the other hand, as expected, Ly6C^{high} monocytes were higher in TNF-α when compared with tissue-resident F4/80^{high}CD169$^+$ macrophages. With the progression of the infection and as a response to the parasite-induced inflammation, activated CD4$^+$

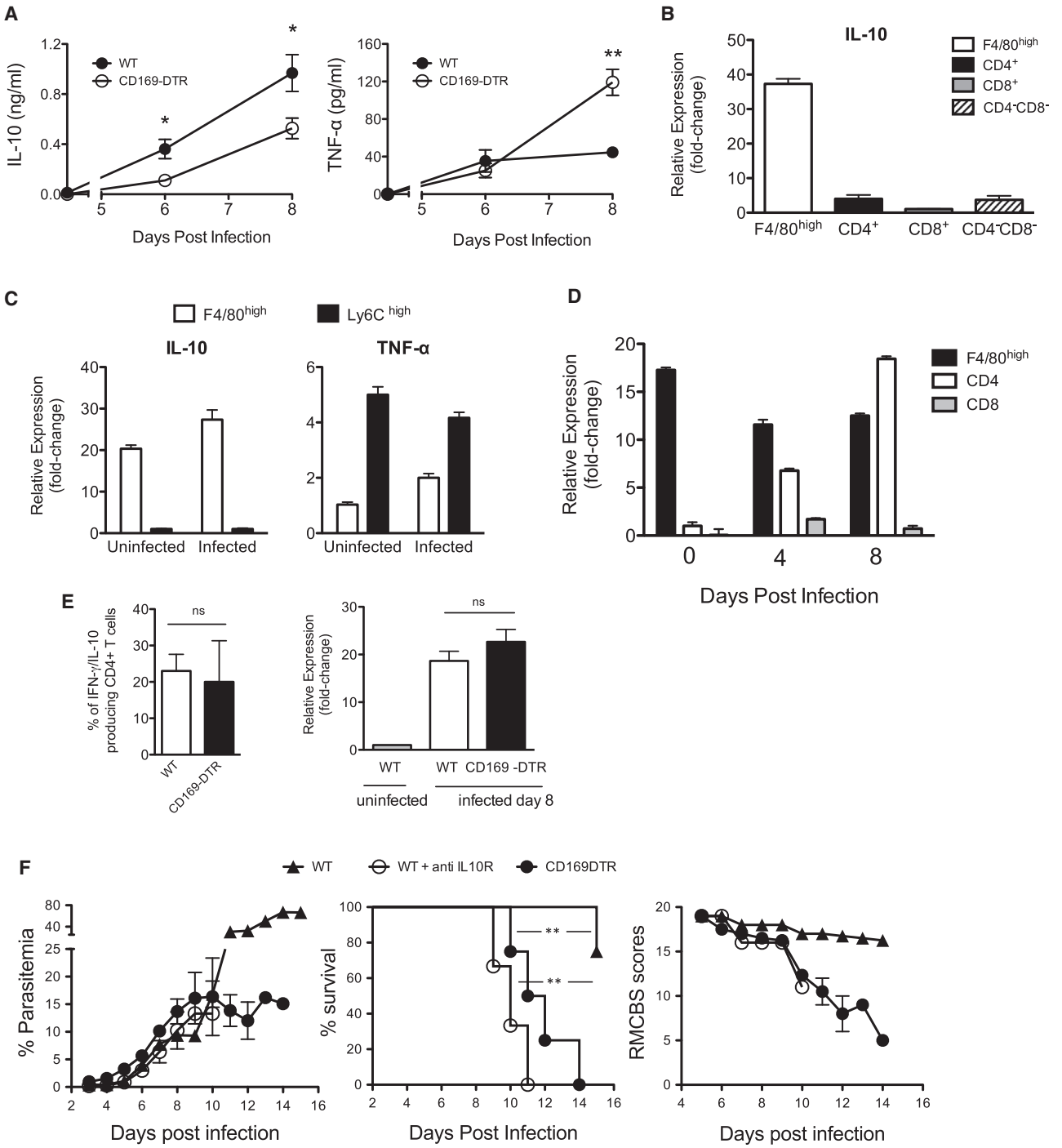

Figure 7. IL-10 and TNF-α Cytokine Levels in WT and CD169-DTR Mice in Steady State and during PbA Infection and Impact of Intervention of IL-10 Signaling to Severity of Infection

(A) Serum IL-10 and TNF-α levels during the course of PbA infection. Mean of IL-10 and TNF-α ± SD measured in the serum of WT and CD169-DTR mice infected with PbA at day 6 and 8 (n = 4–11 mice/group). Statistical significance was determined using an unpaired Student's t test. *p < 0.05.

(B) qPCR analysis of *IL-10* expression in F4/80^{high} macrophages, CD4^{+}, CD8^{+}, and CD4^{-}CD8^{-} T cells isolated from pooled spleens obtained from three uninfected mice. IL-10 and β-actin mRNA levels were measured using real-time PCR. Data were normalized to β-actin and are expressed as fold induction and represented as means of triplicates ± SD.

(C) qPCR analysis of *IL-10* and *TNF-α* expression in F4/80^{high} macrophages and Ly6C^{high} monocytes obtained from livers of control WT mice and PbA-infected mice (day 8). Data are representative of cells collected from three livers in each group.

(legend continued on next page)

T cells became the major contributors to the total IL-10 response with hardly any input from $CD8^+$ T cells (Figure 7D). However, no significant difference in IL-10 secretion (Figure 7E, left panel) as well as in IL-10 mRNA (Figure 7E, right panel) was observed between $CD4^+$ T cells obtained from PbA-infected WT and CD169-DTR mice (day 8), suggesting that the lower IL-10 serum levels measured in CD169-DTR mice were due to the absence of the tissue-resident macrophages.

To test if the reduced serum levels of IL-10 observed in CD169-DTR mice contribute to the PbA-induced immunopathology, we treated WT mice with blocking anti-IL-10R antibody, infected them with PbA, and monitored the parasitemia, survival curve, and ECM susceptibility during 15 days post-infection. Neutralization of the IL-10 activity in WT lead to a similar phenotype observed in CD169-DTR mice in terms of parasitemia profile, rapid lethality, as well as development of clear cerebral malaria signs (Figure 7F).

DISCUSSION

The diverse myeloid cell family, which includes macrophages and dendritic cells (DCs), plays a crucial role in both innate and adaptive host defense during malaria (Chua et al., 2013; Gazzinelli et al., 2014; Wykes et al., 2007). Thus, it is essential that anti-malarial immune responses are tightly controlled and regulated to avoid severe immunopathology that might otherwise arise from excessive and inappropriate immune activation. In the early stages of infection, both DCs and macrophages sense iRBCs through their surface and cytosolic innate receptors. Indeed, toll-like receptors and NOD-like receptors have been shown to recognize parasite-associated products directly, such as glycosylphosphatidylinositol (GPI) anchors, immunostimulatory nucleic acids motifs (Gowda, 2007), and tyrosyl-tRNA synthetase (Bhatt et al., 2011), as well as parasite digestive vacuoles containing Hz (Barrera et al., 2011; Jaramillo et al., 2004; Olivier et al., 2014). Despite their shared role in parasite sensing, DCs and macrophages have distinct functions during the anti-malarial immune response. DCs play a central role in the bridge between innate and adaptive immunity by efficiently presenting malaria-related antigens to naive T cells and initiating protective T and B cell-mediated responses (Langhorne et al., 2004). The major function of macrophages is parasite clearance via phagocytosis, although they are also important for the initiation of an anti-inflammatory response to the parasite infection (Chua et al., 2013; Mac-Daniel and Ménard, 2015). The heterogeneity of the macrophage family, which includes both monocyte-derived and tissue-resident macrophage subsets (Ginhoux and Jung, 2014; Murray and Wynn, 2011), requires that individual subsets are considered separately to understand their individual roles in disease fully. Here, we focused on tissue-resident macrophages, including those in the spleen, lungs, liver, kidneys, heart, and brain (Davies et al., 2013) to dissect their contribution to the control of blood-stage PbA infections.

Tissue-resident macrophages express high levels of the C-type lectin CD169 as well as F4/80 and are often referred to as $F4/80^{hi}$ cells. This subset is distributed in a variety of tissues, such as the spleen (red pulp, marginal zone, and metallophilic macrophages), liver (Kupffer cells), CNS (microglia), lungs (alveolar macrophages), and bones (osteoclasts) (Davies et al., 2013; Murray and Wynn, 2011). $CD169^+F4/80^{hi}$ cells also include vascular-resident macrophages, known as perivascular macrophages (Karasawa et al., 2015). In contrast to monocyte-derived macrophages, which are actively recruited during inflammation (Ginhoux and Jung, 2014), tissue-resident macrophages have the ability to self-renew, maintaining their populations within the tissues (Perdiguero and Geissmann, 2016). Recent fate-mapping experiments have demonstrated that, with the exception of microglia and Langerhans cells, most $F4/80^{hi}$ tissue-resident macrophages are in fact derived from classical hematopoietic stem cells (Sheng et al., 2015). The function of these cells varies according to their tissue localization and can include clearance of senescent and apoptotic cells, regulation of metabolism, bone degradation, surfactant clearance, immune surveillance, initiation of inflammatory responses, as well as restoration of the homeostatic tissue environment (Murray and Wynn, 2011).

We recently generated a CD169-DTR transgenic mouse strain (Purnama et al., 2014), which enables us to ablate tissue-resident macrophages specifically. We have now exploited this animal model to study the contribution of tissue-resident macrophages to the control of immunopathology resulting from PbA infection. During the pathogenesis of malaria, the high parasite burden and resultant activation of inflammatory myeloid cells triggers systemic inflammation, which causes the initial symptoms of the infection. If not tightly controlled, this inflammation can lead to severe complications, such as, cerebral malaria, acute respiratory distress, metabolic acidosis, and clinical jaundice. The potentially fatal consequences of uncontrolled systemic inflammation mean that regulatory mechanisms are of particular importance in malaria.

Here, we demonstrate that tissue-resident macrophages play a crucial role as "brakes" in the early immune response, curbing the potential, and often lethal, runaway effects of acute systemic inflammation. CD169-DTR mice, which lack tissue-resident macrophages, developed an early, but transient peak of parasitemia, which was rapidly followed by the premature death of all PbA-infected mice. In contrast, WT mice survived the initial peak

(D) Time-course analysis of IL-10 expression in $F4/80^{high}$ macrophages, CD4 and CD8 T cells obtained from 3 pooled livers of uninfected (day 0) and infected mice (days 4 and 8). IL-10 mRNA was determined as described above. Data are expressed as means of triplicates ± SD.

(E) Left: detection of IL-10 secreting $CD4^+$ T cells obtained from livers of WT or CD169-DTR mice. Right: intracellular staining of IL-10/IFN-γ (two to three pooled mice ± SD) qPCR analysis of *IL-10* expression in $CD4^+$ T cells isolated and purified from three pooled livers from uninfected WT mice and from PbA-infected WT and CD169-DTR mice (day 8), respectively. IL-10 and β-actin mRNA levels were measured using real-time PCR. Data were normalized to β-actin and are expressed as fold induction and represented as means of triplicates ± SD.

(F) WT BALB/c mice (n = 4) were i.p. injected with anti-IL-10 receptor monoclonal antibody (αIL-10R) or isotype-matched IgG control antibody day −1 before PbA and at day +1, 4, and 7. In parallel, a group of four DT-injected CD169-DTR mice was included. Parasitemia (left), survival (middle), and severity of ECM determined by RMCBS (right) were evaluated. Statistical significance of survival was analyzed using the Mantel-Cox log-rank test. $^{**}p < 0.01$.

of parasitemia but went on to develop steadily increasing levels until they eventually succumbed to the complications of high, chronic parasite loads. The organs of CD169-DTR mice showed greatly increased sequestration of iRBCs together with Hz accumulation, indicative of active infection, and vascular occlusion and leakage. This was accompanied by augmented cell infiltrates of inflammatory-monocytes and neutrophils, hence the premature death of CD169-DTR mice was therefore very likely due to systemic runaway inflammation and multiple organ damage. Similar premature deaths were also observed when CD169-DTR mice were infected with non-lethal *P. yoelii* 17XNL and *P. chabaudi* (unpublished data), suggesting that tissue-resident macrophages are crucial for generating a balanced immune response to malaria parasites and perhaps even to other blood-borne pathogens.

The tissue damage resulting from a lack of $CD169^+$ macrophages appears to be unrelated to the presence of IFN-γ^+ producing $CD4^+$ and $CD8^+$ T cells because IFN-γ^+ responses in these organs were comparable or even reduced in CD169-DTR mice. The observed reduction in the numbers of cytokine-producing T cells in the CD169-DTR model can be explained by the putative antigen presentation capacity of $CD169^+$ macrophages (Martinez-Pomares and Gordon, 2012). The strategic localization of tissue-resident macrophages at sites permanently exposed to blood highlights their contribution in *Plasmodium* uptake, malarial antigen presentation, and subsequent $CD8^+$ T cell activation. Indeed, numerous reports have previously demonstrated the capacity of $CD169^+$ macrophages to cross-present antigen and prime CTL responses (Asano et al., 2011; Backer et al., 2010; Bernhard et al., 2015; Martinez-Pomares and Gordon, 2012). Notably, we observed increased numbers of activated cytokine-producing T cells only in the brains of CD169-DTR mice, which are likely to have contributed, together with the sequestered parasite, to the observed ECM pathology.

For example, hepatic tissue-resident macrophages, better known as Kupffer cells, are located in the vasculature closely adherent to liver sinusoidal endothelial cells and are therefore continuously exposed to gut-derived bacteria and microbial debris (Bilzer et al., 2006). They are optimally positioned to act as immune sentinels and to capture pathogens (Jenne and Kubes, 2013). Not surprisingly, as we demonstrated here, their absence leads to hepatic PbA accumulation and vascular leakage with severe consequences on liver functionality.

In malaria, Hz, a heme detoxification product of the malaria parasite, plays a crucial role in malaria pathophysiology through its inflammatory properties. At schizont rupture, Hz is released into the circulation inside the parasite digestive vacuole (DV), which is normally removed rapidly via phagocytosis of DVs by macrophages and neutrophils (Barrera et al., 2011), explaining the considerable increase in Hz deposition in the tissues when tissue-resident macrophages were absent. Not surprisingly, a strong correlation between high amounts of Hz and the presence of inflammation and tissue pathology has been noted previously (Olivier et al., 2014). Hz, similar to inorganic crystals made of uric acid, asbestos, and silica, activates the NLRP-3 inflammasome and IL-1β release (Tyberghein et al., 2014). Hz is known to induce severe lung inflammation during malaria-associated ARDS (Deroost et al., 2013). In fact, injection of either *Plasmodium falciparum*-derived or synthetic Hz into malaria-free mice induces the production of local pulmonary inflammatory mediators, such as IL-1β, TNF-α, and MIP-1α and MIP-1β (Sherry et al., 1995). Hz-inducible pro-inflammatory mediators are not restricted to the lungs, but are also detectable in the livers of Hz-injected mice (Jaramillo et al., 2004). Elevated hepatic Hz significantly correlates with hepatic inflammation and liver pathology particularly in the case of *P. chabaudi* AS and, to a lesser extent, in PbA infections (Deroost et al., 2014). The increased Hz deposition observed in the organs of CD169 DTR mice following infection indicates a likely role for Hz in driving the increased systemic inflammation observed here. However, Hz is not the only component of malarial parasites capable of promoting parasite-driven inflammation. Other *Plasmodium* metabolites, such as GPIs (Gowda, 2007) and DNA (Gowda et al., 2011; Sharma et al., 2011), can also stimulate the secretion of pro-inflammatory cytokines (Schofield, 2007), which should also be considered.

Every infection, including malaria, has to be tightly controlled through well-balanced effector and regulatory immune responses. As shown here, in absence of tissue-resident $CD169^+$ macrophages this essential balance between parasite-mediated inflammatory and anti-inflammatory responses is perturbed and the resultant low IL-10/TNF ratio in CD169-DTR mice could be one of the possible reasons causing the exacerbated inflammation during PbA infection. IL-10, as key immunoregulator (Couper et al., 2008a), prevents parasite tissue sequestration (Amante et al., 2010; Brugat et al., 2014; Sanni et al., 2004), modulates parasite clearance, and ameliorates immunopathology caused by PbA (Kossodo et al., 1997), by *P. yoelii* (Couper et al., 2008b), as well as by *P. chabaudi chabaudi* (Li et al., 1999; Linke et al., 1996) infections. $CD169^+$ macrophages capable in producing IL-10 especially early during the infection can effectively contribute in regulating the inflammatory response to malaria and thus restrain excessive immunopathology.

In summary, we demonstrate that tissue-resident macrophages, strategically positioned at entry sites of the parasite, play a fundamental role in balancing an optimal immune response to the blood-stage malaria parasite. In their absence, *Plasmodium* parasites are able to trigger a systemic, runaway inflammatory response with marked iRBC sequestration into the tissues, ultimately leading to multiple organ damage, including cerebral pathology and death. Therefore, clinical measures that aim to support the function of these cells should be considered for the development of improved malaria therapies.

EXPERIMENTAL PROCEDURES

Mice and Ethics Statement

The BALB/c CD169-DTR transgenic line was generated as described previously (Purnama et al., 2014) and maintained together with wild-type (WT) BALB/c in the animal facility of Nanyang Technological University of Singapore. Age- and sex-matched animals were used for both strains of mice. They are referred as WT and CD169-DTR mice throughout the text. This study was carried out in strict accordance with the recommendations of the National Advisory Committee for Laboratory Animal Research (NACLAR) guidelines under the Animal and Birds (Care and Use of Animals for Scientific Purposes) Rules of Singapore. The Institutional Animal Care and Use

Committee (IACUC) of the Nanyang Technological University of Singapore (IACUC SBS/NIE A-0127) approved the protocol.

Depletion of Tissue-Resident Macrophages

WT BALB/c and CD169-DTR mice were injected intraperitoneally (i.p.) at day −2 and −1 with 10 ng/g DT, followed by repeat injections every 3–4 days to ensure that depletion of the target cell subpopulation was maintained throughout the experimental phase.

Parasite Strain, Infection Protocol, and Disease Assessment

Transgenic *Plasmodium berghei* ANKA clone 15Cy1-expressing GFP (PbAGFP) (Janse et al., 2006) or clone 231c11-expressing luciferase enzyme (PbAluc) (Franke-Fayard et al., 2005) were used for infection. Both WT and CD169-DTR mice (6–10 weeks old) were injected i.p. with 10^6 iRBCs. Parasitemia and animal survival were monitored over a period of 25 days. Mice were monitored for experimental cerebral malaria every day using the RMCBS score, as previously described (Carroll et al., 2010). For studies involving the in vivo neutralization of IL-10, 200 μg/mouse anti IL-10 R-blocking antibody (BioXCel) was injected at day −1 prior to PbA infection and subsequently day +4 and +7 post infection.

Measurement of Parasite Sequestration

WT and CD169-DTR mice were injected with 10^6 RBCs infected with PbAluc. Parasite sequestration was evaluated from day 6–9 post infection. The mice were anaesthetized with ketamine and xylazine prior to an i.p. injection of 200 μl of D-luciferin potassium salt (Caliper Life Sciences), reconstituted in PBS at a concentration of 5 mg/ml. Mice were sacrificed after 2 min and then intracardially perfused with PBS. Organs (spleen, brain, liver, lungs, kidneys, and heart) were removed immediately for subsequent ex vivo imaging using the IVIS Spectrum CT imaging system (Caliper Life Sciences). Imaging was performed with a 13.6 cm field of view, medium binning factor, and auto exposure settings. Bioluminescence was quantified on the regions of interest by calculating the average radiance in p/s/cm^2/sr using Living Image software version 4.3.1.

Isolation of Leukocytes from Spleen, Brain, Liver, Kidneys, Heart, and Lungs

Spleen single cell suspensions were obtained as described previously (Ruedl et al., 1999). For sequestered leukocyte analysis, mice were first intracardially perfused with PBS. Brain, lungs, kidneys, heart, and livers were then digested with collagenase and single cell suspensions were obtained as described previously (Sheng et al., 2015).

Flow Cytometry, Cell Sorting, and Intracellular Cytokine Staining

Fluorochrome-labeled anti-mouse-CD45, anti-mouse-CD4, anti-mouse-CD8, anti-mouse-CD11b, anti-mouse-F4/80, anti-mouse-Ly6C, and anti-mouse-Ly6G antibodies were purchased from BioLegend. Stained cells were analyzed on a Fortessa FACS (BD Biosciences), and data were analyzed with FlowJo software (TreeStar). The cell sorting was carried out on a BD FACS Aria instrument (gating strategies and purity are shown in Figure S5).

For intracellular IFN-γ staining, isolated spleen, brain, liver, and lung T cells were stimulated with Brefeldin A for 2 hr and stained with anti-CD45-, anti-CD4-, and anti-CD8-specific antibodies. For intracellular IL-10 staining, cells were incubated 2 hr with PMA/Ionomycin before the addition of Brefeldin A. Subsequently, cells were permeabilized and fixed using the FOXP3 Staining Buffer Set according to the manufacturer's instructions (eBioscience) and stained intracellularly with anti-IFN-γ, anti-IL-10, or anti-Granzyme B antibodies (BioLegend). Gating strategies are shown in Figure S5.

Histological Analysis

Brain, liver, kidneys, heart, and lungs were dissected from infected WT and CD169-DTR mice and fixed in 4% phosphate-buffered paraformaldehyde for 48 hr, dehydrated, and embedded in paraffin. Sections (6 μm) were stained with H&E, or with picrosirius red for collagen visualization, and analyzed by bright field light microscopy at 4×, 20×, and 100× magnifications. Images were obtained using a Nikon Eclipse 80i microscope.

Immunofluorescence Cell Staining

For immunofluorescence staining, spleens were removed, cryopreserved by embedding in Optimal Cutting Temperature (O.C.T.) compound (Tissue Tek), and stored at −80°C. Sections (6 μm) were cut and thawed for 20 min at room temperature, and acetone-fixed for 10 min. The sections were then incubated with FITC-labeled anti-CD169 and biotinylated anti-SIGN-R1 antibodies or Texas Red-labeled anti-CD169 together with FITC-labeled CD31 (4°C overnight). After washing with PBS, the sections were stained for an additional hour with Texas Red-labeled streptavidin and mounted with DAKO fluorescent mounting medium. Images were obtained using a Nikon Eclipse 80i microscope at 20× magnification.

Alanine Aminotransferase Assay

Liver damage was quantified by measuring alanine aminotransferase (ALT) in the serum using a MaxDiscovery Alanine Transaminase (ALT) Enzymatic Assay Kit (Bio Scientific) following the manufacturer's instructions.

ELISA Measurement of IgM and IgG in BAL Fluid

A sandwich ELISA was used to measure total mouse IgG and IgM levels in BAL samples collected from infected WT or CD169-DTR mice. In brief, 96-well ELISA plates (Nunc, Maxisorp) were coated overnight with 100 μl of a 1:400 dilution of either goat anti–mouse IgG or IgM (Southern Biotech) antibody in PBS. After a blocking step with 2% bovine calf serum in PBS, plates were incubated overnight at 4°C with collected BAL samples. A 1:3,000 dilution of the appropriate conjugate (HRP conjugated anti-IgG or anti-IgM antibodies; Southern Biotech) was added to each well for 1 hr. The plates were washed and incubated with TMB substrate (BioLegend) for 10 min. The water-soluble blue reaction product was measured spectrophotometrically at 370 nm.

ELISA Measurement of Serum Cytokines

Serum IFN-γ, TNF-α, and IL-10 levels were quantified using the appropriate ELISA MAX Standard kit (BioLegend) according to the manufacturer's instructions.

Measurement of Blood-Brain Barrier Integrity

Blood-brain barrier (BBB) permeability was assessed by intravenously injecting 200 μl of 1% Evans blue/PBS into PbA-infected WT and CD169-DTR mice. The animals were sacrificed 1 hr later and perfused intracardially with PBS. Brains were collected, weighed, and placed in 1 ml of 100% formamide for 48 hr to extract the Evans blue dye from the tissue. Absorbance of the formamide extraction was then measured at 620 nm and normalized by the weight of the tissue.

Hemorrhage and Hz Quantification

The numbers of hemorrhagic foci in the brain parenchyma were manually counted per brain section under 20× magnification. Hz deposits were quantified using the HistoQuest program (TissueGnostics USA) as follows: bright field images from at least ten fields of view were acquired at 100× magnification per organ on Nikon Eclipse 80i. The Hz deposit area was quantified and normalized to total cell area in each image using HistoQuest. Each data point represents these normalized hemozoin deposits area values quantified from single fields of view.

Quantitative Real-Time PCR

qPCR was performed on cDNA obtained from sorted cells using SYBR green chemistry (KabaBiosystem). Reactions were run on a real-time qPCR system (Illumina). Samples were normalized to β-actin, represent the median of triplicate analyses, and are displayed as relative expression. Primer sequences were as follows: *IL-10*, Fwd: 5′-CAGAGCCACATGCTCCTAGA-3′, Rev: 5′-TGTCCAGCTGGTCCTTTGTT-3′; *TNF-α*, Fwd: 5′-AATTCGAGTGACAAG CCTGTAG-3′, Rev: 5′-TTGAGATCCATGCCGTTGG-3′; and *β-Actin*, Fwd: 5′-AAGGCCAACCGTGAAAAGAT-3′, Rev: 5′-CCTGTGGTACGACCAGAGG CATACA-3′.

Statistical Analysis

Survival was analyzed using the Mantel-Cox log-rank test. Statistical significance between two groups was analyzed using the unpaired Student's t test

or Mann-Whitney U test and for more than two groups using an one-way ANOVA followed by Bonferroni test. Statistical significance is demonstrated in the figures with asterisks: *p < 0.05, **p < 0.01, ***p < 0.001, ****p < 0.0001. GraphPad Prism 5.0 was used to analyze the data.

SUPPLEMENTAL INFORMATION

Supplemental Information includes five figures and can be found with this article online at http://dx.doi.org/10.1016/j.celrep.2016.07.010.

AUTHOR CONTRIBUTIONS

P.G. performed the experiments and analyzed the data. S.M.L., P.T., A.B., and J.S. contributed to specific experiments. C.C, L.R., and K.K. provided experimental guidance and expertise. C.R. conceived the study, designed the experiments, analyzed and interpreted the data, and wrote the manuscript.

ACKNOWLEDGMENTS

We thank Monika Tetlak and Yolanda Setiagiani for excellent technical support. We would like to thank the Advanced Molecular Pathology Laboratory team and Dr. Muthafar Al-Addawi (IMCB, A*Star) for the excellent histopathological evaluation. We would like to thank Kerry McLaughlin of Insight Editing London for critical review of the manuscript. This work was supported by National Medical Research Council grants NMRC 1253/2010 and NMRC/1307/2011 to C.R. Part of this work was supported by core grants to the Singapore Immunology Network from Agency for Science, Technology and Research (A*STAR).

Received: October 19, 2015
Revised: May 23, 2016
Accepted: July 1, 2016
Published: July 28, 2016

REFERENCES

Amante, F.H., Haque, A., Stanley, A.C., Rivera, Fde.L., Randall, L.M., Wilson, Y.A., Yeo, G., Pieper, C., Crabb, B.S., de Koning-Ward, T.F., et al. (2010). Immune-mediated mechanisms of parasite tissue sequestration during experimental cerebral malaria. J. Immunol. *185*, 3632–3642.

Asano, K., Nabeyama, A., Miyake, Y., Qiu, C.H., Kurita, A., Tomura, M., Kanagawa, O., Fujii, S., and Tanaka, M. (2011). CD169-positive macrophages dominate antitumor immunity by crosspresenting dead cell-associated antigens. Immunity *34*, 85–95.

Bach, O., Baier, M., Pullwitt, A., Fosiko, N., Chagaluka, G., Kalima, M., Pfister, W., Straube, E., and Molyneux, M. (2005). Falciparum malaria after splenectomy: a prospective controlled study of 33 previously splenectomized Malawian adults. Trans. R. Soc. Trop. Med. Hyg. *99*, 861–867.

Backer, R., Schwandt, T., Greuter, M., Oosting, M., Jüngerkes, F., Tüting, T., Boon, L., O'Toole, T., Kraal, G., Limmer, A., and den Haan, J.M. (2010). Effective collaboration between marginal metallophilic macrophages and CD8+ dendritic cells in the generation of cytotoxic T cells. Proc. Natl. Acad. Sci. USA *107*, 216–221.

Barrera, V., Skorokhod, O.A., Baci, D., Gremo, G., Arese, P., and Schwarzer, E. (2011). Host fibrinogen stably bound to hemozoin rapidly activates monocytes via TLR-4 and CD11b/CD18-integrin: a new paradigm of hemozoin action. Blood *117*, 5674–5682.

Bernhard, C.A., Ried, C., Kochanek, S., and Brocker, T. (2015). CD169+ macrophages are sufficient for priming of CTLs with specificities left out by cross-priming dendritic cells. Proc. Natl. Acad. Sci. USA *112*, 5461–5466.

Bhatt, T.K., Khan, S., Dwivedi, V.P., Banday, M.M., Sharma, A., Chandele, A., Camacho, N., Ribas de Pouplana, L., Wu, Y., Craig, A.G., et al. (2011). Malaria parasite tyrosyl-tRNA synthetase secretion triggers pro-inflammatory responses. Nat. Commun. *2*, 530.

Bilzer, M., Roggel, F., and Gerbes, A.L. (2006). Role of Kupffer cells in host defense and liver disease. Liver Int. *26*, 1175–1186.

Brugat, T., Cunningham, D., Sodenkamp, J., Coomes, S., Wilson, M., Spence, P.J., Jarra, W., Thompson, J., Scudamore, C., and Langhorne, J. (2014). Sequestration and histopathology in Plasmodium chabaudi malaria are influenced by the immune response in an organ-specific manner. Cell. Microbiol. *16*, 687–700.

Carroll, R.W., Wainwright, M.S., Kim, K.Y., Kidambi, T., Gómez, N.D., Taylor, T., and Haldar, K. (2010). A rapid murine coma and behavior scale for quantitative assessment of murine cerebral malaria. PLoS ONE *5*, e13124.

Chua, C.L., Brown, G., Hamilton, J.A., Rogerson, S., and Boeuf, P. (2013). Monocytes and macrophages in malaria: protection or pathology? Trends Parasitol. *29*, 26–34.

Claser, C., Malleret, B., Gun, S.Y., Wong, A.Y., Chang, Z.W., Teo, P., See, P.C., Howland, S.W., Ginhoux, F., and Rénia, L. (2011). CD8+ T cells and IFN-γ mediate the time-dependent accumulation of infected red blood cells in deep organs during experimental cerebral malaria. PLoS ONE *6*, e18720.

Cockburn, I.A., and Zavala, F. (2016). Dendritic cell function and antigen presentation in malaria. Curr. Opin. Immunol. *40*, 1–6.

Cooke, B.M., Mohandas, N., and Coppel, R.L. (2004). Malaria and the red blood cell membrane. Semin. Hematol. *41*, 173–188.

Couper, K.N., Blount, D.G., and Riley, E.M. (2008a). IL-10: the master regulator of immunity to infection. J. Immunol. *180*, 5771–5777.

Couper, K.N., Blount, D.G., Wilson, M.S., Hafalla, J.C., Belkaid, Y., Kamanaka, M., Flavell, R.A., de Souza, J.B., and Riley, E.M. (2008b). IL-10 from CD4CD25Foxp3CD127 adaptive regulatory T cells modulates parasite clearance and pathology during malaria infection. PLoS Pathog. *4*, e1000004.

Davies, L.C., Jenkins, S.J., Allen, J.E., and Taylor, P.R. (2013). Tissue-resident macrophages. Nat. Immunol. *14*, 986–995.

Deroost, K., Tyberghein, A., Lays, N., Noppen, S., Schwarzer, E., Vanstreels, E., Komuta, M., Prato, M., Lin, J.W., Pamplona, A., et al. (2013). Hemozoin induces lung inflammation and correlates with malaria-associated acute respiratory distress syndrome. Am. J. Respir. Cell Mol. Biol. *48*, 589–600.

Deroost, K., Lays, N., Pham, T.T., Baci, D., Van den Eynde, K., Komuta, M., Prato, M., Roskams, T., Schwarzer, E., Opdenakker, G., and Van den Steen, P.E. (2014). Hemozoin induces hepatic inflammation in mice and is differentially associated with liver pathology depending on the Plasmodium strain. PLoS ONE *9*, e113519.

Engwerda, C., Belnoue, E., Grüner, A.C., and Rénia, L. (2005a). Experimental models of cerebral malaria. Curr. Top. Microbiol. Immunol. *297*, 103–143.

Engwerda, C.R., Beattie, L., and Amante, F.H. (2005b). The importance of the spleen in malaria. Trends Parasitol. *21*, 75–80.

Franke-Fayard, B., Janse, C.J., Cunha-Rodrigues, M., Ramesar, J., Büscher, P., Que, I., Löwik, C., Voshol, P.J., den Boer, M.A., van Duinen, S.G., et al. (2005). Murine malaria parasite sequestration: CD36 is the major receptor, but cerebral pathology is unlinked to sequestration. Proc. Natl. Acad. Sci. USA *102*, 11468–11473.

Gazzinelli, R.T., Kalantari, P., Fitzgerald, K.A., and Golenbock, D.T. (2014). Innate sensing of malaria parasites. Nat. Rev. Immunol. *14*, 744–757.

Ginhoux, F., and Jung, S. (2014). Monocytes and macrophages: developmental pathways and tissue homeostasis. Nat. Rev. Immunol. *14*, 392–404.

Gowda, D.C. (2007). TLR-mediated cell signaling by malaria GPIs. Trends Parasitol. *23*, 596–604.

Gowda, N.M., Wu, X., and Gowda, D.C. (2011). The nucleosome (histone-DNA complex) is the TLR9-specific immunostimulatory component of Plasmodium falciparum that activates DCs. PLoS ONE *6*, e20398.

Janse, C.J., Franke-Fayard, B., and Waters, A.P. (2006). Selection by flow-sorting of genetically transformed, GFP-expressing blood stages of the rodent malaria parasite, Plasmodium berghei. Nat. Protoc. *1*, 614–623.

Jaramillo, M., Plante, I., Ouellet, N., Vandal, K., Tessier, P.A., and Olivier, M. (2004). Hemozoin-inducible proinflammatory events in vivo: potential role in malaria infection. J. Immunol. *172*, 3101–3110.

Jenne, C.N., and Kubes, P. (2013). Immune surveillance by the liver. Nat. Immunol. *14*, 996–1006.

Karasawa, K., Asano, K., Moriyama, S., Ushiki, M., Monya, M., Iida, M., Kuboki, E., Yagita, H., Uchida, K., Nitta, K., and Tanaka, M. (2015). Vascular-resident CD169-positive monocytes and macrophages control neutrophil accumulation in the kidney with ischemia-reperfusion injury. J. Am. Soc. Nephrol. *26*, 896–906.

Kossodo, S., Monso, C., Juillard, P., Velu, T., Goldman, M., and Grau, G.E. (1997). Interleukin-10 modulates susceptibility in experimental cerebral malaria. Immunology *91*, 536–540.

Langhorne, J., Albano, F.R., Hensmann, M., Sanni, L., Cadman, E., Voisine, C., and Sponaas, A.M. (2004). Dendritic cells, pro-inflammatory responses, and antigen presentation in a rodent malaria infection. Immunol. Rev. *201*, 35–47.

Li, C., Corraliza, I., and Langhorne, J. (1999). A defect in interleukin-10 leads to enhanced malarial disease in Plasmodium chabaudi chabaudi infection in mice. Infect. Immun. *67*, 4435–4442.

Linke, A., Kühn, R., Müller, W., Honarvar, N., Li, C., and Langhorne, J. (1996). Plasmodium chabaudi chabaudi: differential susceptibility of gene-targeted mice deficient in IL-10 to an erythrocytic-stage infection. Exp. Parasitol. *84*, 253–263.

Mac-Daniel, L., and Ménard, R. (2015). Plasmodium and mononuclear phagocytes. Microb. Pathog. *78*, 43–51.

Martinez-Pomares, L., and Gordon, S. (2012). CD169+ macrophages at the crossroads of antigen presentation. Trends Immunol. *33*, 66–70.

Murray, P.J., and Wynn, T.A. (2011). Protective and pathogenic functions of macrophage subsets. Nat. Rev. Immunol. *11*, 723–737.

Murthi, P., Kalionis, B., Ghabrial, H., Dunlop, M.E., Smallwood, R.A., and Sewell, R.B. (2006). Kupffer cell function during the erythocytic stage of malaria. J. Gastroenterol. Hepatol. *21*, 313–318.

Olivier, M., Van Den Ham, K., Shio, M.T., Kassa, F.A., and Fougeray, S. (2014). Malarial pigment hemozoin and the innate inflammatory response. Front. Immunol. *5*, 25.

Perdiguero, E.G., and Geissmann, F. (2016). The development and maintenance of resident macrophages. Nat. Immunol. *17*, 2–8.

Piva, L., Tetlak, P., Claser, C., Karjalainen, K., Renia, L., and Ruedl, C. (2012). Cutting edge: Clec9A+ dendritic cells mediate the development of experimental cerebral malaria. J. Immunol. *189*, 1128–1132.

Purnama, C., Ng, S.L., Tetlak, P., Setiagani, Y.A., Kandasamy, M., Baalasubramanian, S., Karjalainen, K., and Ruedl, C. (2014). Transient ablation of alveolar macrophages leads to massive pathology of influenza infection without affecting cellular adaptive immunity. Eur. J. Immunol. *44*, 2003–2012.

Ruedl, C., Kopf, M., and Bachmann, M.F. (1999). CD8(+) T cells mediate CD40-independent maturation of dendritic cells in vivo. J. Exp. Med. *189*, 1875–1884.

Sanni, L.A., Jarra, W., Li, C., and Langhorne, J. (2004). Cerebral edema and cerebral hemorrhages in interleukin-10-deficient mice infected with Plasmodium chabaudi. Infect. Immun. *72*, 3054–3058.

Schofield, L. (2007). Intravascular infiltrates and organ-specific inflammation in malaria pathogenesis. Immunol. Cell Biol. *85*, 130–137.

Schofield, L., and Grau, G.E. (2005). Immunological processes in malaria pathogenesis. Nat. Rev. Immunol. *5*, 722–735.

Schulz, C., Gomez Perdiguero, E., Chorro, L., Szabo-Rogers, H., Cagnard, N., Kierdorf, K., Prinz, M., Wu, B., Jacobsen, S.E., Pollard, J.W., et al. (2012). A lineage of myeloid cells independent of Myb and hematopoietic stem cells. Science *336*, 86–90.

Sharma, S., DeOliveira, R.B., Kalantari, P., Parroche, P., Goutagny, N., Jiang, Z., Chan, J., Bartholomeu, D.C., Lauw, F., Hall, J.P., et al. (2011). Innate immune recognition of an AT-rich stem-loop DNA motif in the Plasmodium falciparum genome. Immunity *35*, 194–207.

Sheng, J., Ruedl, C., and Karjalainen, K. (2015). Most Tissue-Resident Macrophages Except Microglia Are Derived from Fetal Hematopoietic Stem Cells. Immunity *43*, 382–393.

Sherman, I.W., Eda, S., and Winograd, E. (2004). Erythrocyte aging and malaria. Cell. Mol. Biol. (Noisy-le-grand) *50*, 159–169.

Sherry, B.A., Alava, G., Tracey, K.J., Martiney, J., Cerami, A., and Slater, A.F. (1995). Malaria-specific metabolite hemozoin mediates the release of several potent endogenous pyrogens (TNF, MIP-1 alpha, and MIP-1 beta) in vitro, and altered thermoregulation in vivo. J. Inflamm. *45*, 85–96.

Sponaas, A.M., Freitas do Rosario, A.P., Voisine, C., Mastelic, B., Thompson, J., Koernig, S., Jarra, W., Renia, L., Mauduit, M., Potocnik, A.J., and Langhorne, J. (2009). Migrating monocytes recruited to the spleen play an important role in control of blood stage malaria. Blood *114*, 5522–5531.

Taylor, W.R., Cañon, V., and White, N.J. (2006). Pulmonary manifestations of malaria : recognition and management. Treat. Respir. Med. *5*, 419–428.

Tyberghein, A., Deroost, K., Schwarzer, E., Arese, P., and Van den Steen, P.E. (2014). Immunopathological effects of malaria pigment or hemozoin and other crystals. Biofactors *40*, 59–78.

Weiss, L. (1989). Mechanisms of splenic control of murine malaria: cellular reactions of the spleen in lethal (strain 17XL) Plasmodium yoelii malaria in BALB/c mice, and the consequences of pre-infective splenectomy. Am. J. Trop. Med. Hyg. *41*, 144–160.

Wunderlich, F., Al-Quraishy, S., and Dkhil, M.A. (2014). Liver-inherent immune system: its role in blood-stage malaria. Front Microbiol *5*, 559.

Wykes, M., Keighley, C., Pinzon-Charry, A., and Good, M.F. (2007). Dendritic cell biology during malaria. Cell. Microbiol. *9*, 300–305.